Radiation-responsive polymers: a novel spectral approach to investigate ultrahigh molecular weight polyethylene modifications using Grünwald-Letnikov and Caputo fractional order derivatives

M. Mudassir Saeed, M. Muddassar, M. Sajjad Mehmood, and N. Siddiqui

Department of Basic Sciences, University of Engineering and Technology, Taxila. 47050, Pakistan

**e-mail: mudassiruet08@gmail.com; muhammad.mudassar@uettaxila.edu.pk; malik.mehmood@uettaxila.edu.pk; nasir.siddiqui@uettaxila.edu.pk*

Received 10 February 2024; accepted 16 August 2024

The impact of gamma radiation on Ultrahigh Molecular Weight Polyethylene (UHMWPE) using fractional differential transformations of FTIR spectra has been probed during the current study. The gamma irradiated samples of UHMWPE for doses of 0, 25, and 50 kGy have been tested with FTIR spectroscopy, and subsequent to testing each spectrum has been analyzed with fraction order differentiation ranging from 0.5 to 1. The exhibited significant shifts in absorbance due to radiation-induced physical and chemical changes, including C=C unsaturation, C=O carbonyl absorption, and variations in CH_2 bending and stretching frequencies are clearly evident even at the lowest order of applied transformation. The weak bands in spectral regions $800 - 1100$ cm^{-1} because of gamma radiation caused peak splitting in the $800 - 1100$ cm^{-1} region, attributed to the conversion of vinyl groups into vinylidene and trans-vinylene groups, have also been observed at all orders of applied transformations. It is, therefore, fractional differential transformations thus proved to be a potential methodology for in depth spectra analysis of radiation responsive polymers like UHMWPE with a minimal information loss during the transformation. This is also confirmed by sensitivity and specificity analysis that demonstrated that lower-order transformations are effective for accurate spectral characterization.

Keywords: Grünwald-Letnikov fractional order derivatives; ATR-FTIR spectroscopy; UHMWPE; principal component analysis; Caputo fractional order derivatives.

DOI: https://doi.org/10.31349/RevMexFis.71.011005

1. Introduction

Due to their affordable manufacture, adaptability, and unique physical and chemical properties, polymer materials, which are made up of lengthy chains of repeating molecular units, have significantly increased in popularity [1-4]. A particular variety of polymer known as ultra-high molecular weight polyethylene (UHMWPE) stands out among the diverse range of polymers. UHMWPE has a molecular weight that is exceptionally high, often between 3 and 6 million grammes per mole. This extraordinary polymer has a wide range of uses, including as an electrical insulator, in the development of artificial implants like joint replacements, and even in the microelectronics sector [5,6]. UHMWPE is capable of undergoing alterations through a technique called crosslinking to improve its characteristics for these many purposes. In crosslinking, the molecular structure of the polymer is changed through the application of various chemical or physical techniques, such as radiation, organo-silane treatments, and the use of peroxides [5-7]. The features and behaviour of the material may be significantly altered by this change, making it better suited for particular uses. The properties and changes of UHMWPE are studied using a variety of analytical techniques. These include differential scanning calorimetry (DSC), X-ray diffraction (XRD), and Fourier transform infrared (FTIR) spectroscopy [7]. Each approach, though, has its limitations. They could have trouble picking up little signals, including faint infrared bands and minute levels of pollutants or toxins. As a result, conclusions drawn from these techniques may not be accurate, which could. The sensitivity and precision of FTIR spectroscopy, which is particularly skilled at examining structural changes in materials after modifications, must be increased through preprocessing. However, there are certain difficulties with FTIR spectroscopy. It might have trouble detecting extremely minute amounts of pollutants and dim infrared spectrum bands. Additionally, the results of FTIR spectroscopy might occasionally be difficult to interpret and unreliable. This results from the method's reliance on measuring the light that travels through or reflects from a sample and later analysing the data gathered. However, this data could contain unwanted noise, such as changes in the baseline of the spectrum and inconsistencies in the signal. These elements could influence how accurately UHMWPE alterations, like those brought on by irradiation, are assessed. Researchers use a preprocessing procedure with the FTIR spectrum data to address these problems and get reliable results. To increase the sensitivity of their analysis and enhance the identification of weak infrared bands, they investigate the use of differential filters in this context, specifically fractional order differential filters. For UHMWPE products to operate better and to be safe in a variety of applications, it is crucial to identify these minute bands and recognise the changes induced by radiation in the material.

The primary purpose of this work is to provide a more accurate and sensitive technique for characterising UHMWPE. The researchers intend to go beyond the limitations of standard approaches by closely examining Attenuated Total Reflection Fourier Transform Infrared (ATR-FTIR) spectra. In FTIR spectroscopy, a sampling method called ATR is employed. The investigation involves comparing the spectra obtained from pristine (unaltered) UHMWPE samples and those that were exposed to gamma radiation. To improve the precision of the analysis, researchers employ fractional order differential filters with varying orders ranging from 0 to 1. These filters aid in the processing of the spectra, the extraction of significant data, and the improvement of the assessment's correctness. The study paper explains how to create simulated spectra using the real experimental data obtained using ATR-FTIR as well as the notion of fractional order derivatives. Researchers use the strength of Principal Component Analysis (PCA) and correlation index analysis to determine the most sensitive and effective transformation. These sophisticated statistical methods make it easier to understand the links and patterns found in intricate datasets. The analysis in this paper also makes use of Caputo fractional derivatives, a mathematical technique for studying complicated systems with fractional order behaviour, which the researchers say is powerful. Researchers can examine the complex spectrum variations in the experimental data by using Caputo fractional derivatives. This method makes it possible to comprehend radiation-induced changes in UHMWPE polymer samples better. A thorough investigation of the material's response gamma radiation is possible because to the use of both experimental spectra and spectra produced using fractional order differentiation, which increases the analysis's robustness. This dual-spectrum study sheds important light on the minute changes in UHMWPE samples.

The main goal of this investigation is to thoroughly evaluate the gamma radiation-induced changes to UHMWPE. Finally, the purpose of this research is to give a full and sophisticated understanding of UHMWPE and its variations. The researchers hope to unearth priceless insights that can greatly contribute to the innovation and safety of polymer-based products across a wide spectrum of applications by painstakingly analysing the spectral data using cutting-edge mathematical methodologies.

2. Background literature

L'Hospital asked Leibniz for clarification in 1695 regarding the meaning of the statement $d^n y/dx^n$ when n is equal to $1/2$. Leibniz responded on September 30, 1695, saying that this hypothetical situation would initially result in uncertainty but would ultimately produce favourable results. This discussion set the way for the creation of Fractional Calculus, a completely new branch of mathematics. This field investigates the integration and differentiation of non-integer orders. Lacroix, who introduced the idea of fractional derivatives for the first time in 1819, made a substantial contribution to this field. He introduced a formula involving the gamma function and constants that became a key concept in comprehending how fractional derivatives behave. L'Hospital's inquiry and Leibniz's response set off an investigation that led to the development of fractional calculus. The focus of this area, sometimes known as fractional calculus, is the application of conventional calculus ideas to non-integer orders. With values that fall between integer increments, it offers a novel viewpoint on how functions evolve and integrate. The contribution made in 1819 by Lacroix developed this concept. He offered a method that could represent and calculate fractional derivatives while accommodating non-integer orders of differentiation [8,9]. This signified a substantial improvement in our understanding of mathematics and created opportunities for applications in other fields. In essence, the historical conversation between Leibniz and L'Hospital set the stage for a new field of mathematics called fractional calculus. Since then, this discipline has demonstrated its importance by providing:

$$\frac{d^{\frac{1}{2}}}{d\xi^{\frac{1}{2}}}\left(\xi^{c}\right)=\frac{\Gamma(c+1)}{\Gamma(c+\frac{1}{2})}\xi^{\left(c-\frac{1}{2}\right)}. \tag{1}$$

The expression $d^{1/2}/d\xi^{1/2}$ represents the fractional derivative operator of order $1/2$. The symbol Γ represents the gamma function, and the letter c stands for a constant. This concept was then extended to provide a detailed representation of $f(\xi)$ using the Fourier method.

$$f(\xi)=\frac{1}{2\pi}\int_{-\infty}^{\infty}f(\rho)d\rho\int_{-\infty}^{\infty}\cos\theta(\xi-\rho)d\theta. \tag{2}$$

With the variables ξ and ρ, the above representation allows us to define the concept of a fractional derivative of order β for a function $f(\xi)$ in the following way:

$$\frac{d^{\beta}f(\xi)}{d\xi^{\beta}}=\frac{1}{2\pi}\int_{-\infty}^{\infty}f(\rho)\,d\rho\int_{-\infty}^{\infty}\theta^{\beta}\times\cos\left(\theta(\xi-\rho)+\beta\frac{\pi}{2}\right)d\theta, \tag{3}$$

where β is a random constant. We employ this fractional calculus definition to address a composite equation that emerges from the tautochrone problem. In this problem, our objective is to ascertain an unidentified function, denoted as $f(\gamma)$, through the evaluation of the subsequent integral:

$$k=\int_{0}^{x}(\xi-\gamma)^{\alpha}f(\gamma)\,d\gamma. \tag{4}$$

In the context where $d^{1/2}/d\xi^{1/2}$ represents a fractional derivative operator with an order of $1/2$, it is important to note that, under specific conditions for $f(\xi)$, fractional operators exhibit the following property:

$$\frac{d^{\frac{1}{2}}}{d\xi^{\frac{1}{2}}}\left[\frac{d^{-\frac{1}{2}}f(\xi)}{d\xi^{-\frac{1}{2}}}\right]=\frac{d^{0}f(\xi)}{d\xi^{0}}=f(\xi). \tag{5}$$

Liouville [10-12] offered the first explicit definition of partial differentiation in 1832. Liouville turned the function $f(\xi)$ into a series and proposed that for order numbers β at which the series transitions, the following statement stays true.

$$f(\xi) = \sum_{n=0}^{\infty} p_n e^{q_n \xi}, \tag{6}$$

and assuming that

$$D^{\beta} f(\xi) = \sum_{n=0}^{\infty} p_n q_n^{\beta} e^{q_n \xi}. \tag{7}$$

In this context, where D^{β} represents the fractional derivative operator with order β and e represents the exponential function, it was later developed by two mathematicians, Grünwald and Letnikov. This method provides a way to compute fractional derivatives by approximating them as a limit of a finite difference quotient.

$$D^{\beta} f(\xi) = \lim_{h \to 0} \frac{1}{h^{\beta}} \sum_{k=0}^{\infty} (-1)^k \binom{\beta}{k} f(\xi - kh). \tag{8}$$

Although fractional calculus has been discussed in books for almost three centuries, its actual applications have only lately come to light. Many scientists are currently actively investigating the use of fractional calculus in a variety of domains.

2.1. Fractional order derivatives definitions

Mathematical operators known as fractional derivatives extend the notion of differentiation to non-integer orders. Fractional derivatives allow us to differentiate a function to a non-integer order, while regular derivatives only work with whole integers (*e.g.*, first derivative, second derivative). They have uses in physics, engineering, and signal processing, among other disciplines. I'll outline a few of the definitions and methods used to define fractional derivatives below.

2.1.1. Riemann-Liouville fractional order derivatives

The Riemann-Liouville fractional integral operator extends the concept of Cauchy's formula to encompass multiple integrations.

$$\int_a^x d\eta \int_a^{x_1} d\eta \ldots \int_a^{x_{n-1}} f(\eta) d\eta = \frac{1}{(n-1)!} \int_a^x \frac{f(\eta)}{(x-\eta)^{1-n}} d\eta. \tag{9}$$

If $f(\eta) \in C[a,b]$ and $\alpha > 0$, then

$$I^{\alpha}_{(a^+)} f(x) = \frac{1}{\Gamma(\alpha)} \int_a^x \frac{f(\eta)}{(x-\eta)^{1-\alpha}} d\eta, \quad x > a, \tag{10}$$

$$I^{\alpha}_{(b^-)} f(x) = \frac{1}{\Gamma(\alpha)} \int_x^b \frac{f(\eta)}{(\eta-x)^{1-\alpha}} d\eta, \quad x < b, \tag{11}$$

are known as the left-sided and right-sided Riemann-Liouville fractional integrals of order α.

Definition 1. *L*et $\alpha \in (0,1)$. The fractional derivative of Riemann-Liouville of order α is given by:

$$D^{\alpha}_a f(x) = \frac{1}{\Gamma(1-\alpha)} \frac{d}{dx} \times \int_a^x \frac{f(\eta)}{(x-\eta)^{\alpha}} d\eta = D I^{1-\alpha}_a f(x). \tag{12}$$

This expression represents the left-sided fractional derivative. When considering the right-sided fractional derivative, the fractional derivative of Riemann-Liouville of order α is used.

Definition 2. *L*et $n-1 < \alpha \leq n$ then for order, the left and right-sided Riemann-Liouville fractional derivatives are defined as:

$$D^{\alpha}_{a^+} f(x) = \frac{1}{\Gamma(1-\alpha)} \frac{d^n}{dx^n} \int_a^x \frac{f(\eta)}{(x-\eta)^{\alpha+1-n}} d\eta = D^n I^{n-\alpha}_{a^+} f(x); x > a, \tag{13}$$

$$D^{\alpha}_{b^-} f(x) = \frac{1}{\Gamma(1-\alpha)} \frac{d^n}{dx^n} \int_x^b \frac{f(\eta)}{(x-\eta)^{\alpha+1-n}} d\eta = D^n I^{n-\alpha}_{b^-} f(x); x < b. \tag{14}$$

Constant's fractional order Riemann-Liouville derivative is not zero.

$$D^{\alpha} C = \frac{C \eta^{-\alpha}}{\Gamma(1-\alpha)} \neq 0. \tag{15}$$

An initial value problem (IVP) with a Riemann-Liouville fractional derivative must have the following initial conditions: $D^{(\alpha-j)} f(0)$, *i.e.*,

$$I^{\alpha} \left(D^{\alpha} f(\eta) \right) = f(\eta) - \sum_{j=1}^{n} \frac{D^{(\alpha-j)} f(0)\, \eta^{(\alpha-j)}}{\Gamma(\alpha - j + 1)}, \tag{16}$$

where $n-1 \leq \alpha < n$.

M. Caputo presented a fresh derivative concept to solve these restrictions that make it impracticable to describe real-world events. This method can be used to create the starting conditions for fractional initial value problems (IVPs) by employing only the boundary values of full-order derivatives at the lower terminal.

2.1.2. Grünwald-Letnikov fractional order derivative

The Grünwald-Letnikov fractional derivative, which is a powerful tool for numerically approximating fractional derivatives of functions, is used in many disciplines [13]. The modelling of systems with non-integer order dynamics, like viscoelastic materials and anomalous diffusion processes, is made possible by its widespread use in numerical computation. This method is advantageous for the study of fractals and fractal geometry, fractional control systems, fractional

differential equations in physics and engineering, and fractals. The Grünwald-Letnikov fractional derivative offers a flexible method for capturing non-integer order phenomena and memory effects in mathematical models and simulations, whether describing complex behaviours in heat conduction, operating robotic systems, studying the spread of pollutants, or looking into fractal patterns in nature. The limit of the Grünwald-Letnikov fractional derivative involves a finite difference quotient. The succeeding differentiation of the function $f(t)$ are expressed as follows

$$f^{(1)}(\eta) = \lim_{h\to 0} \frac{f(\eta+h)-f(\eta)}{h}, \tag{17}$$

$$\begin{aligned} f^{(2)}(\eta) &= \lim_{h\to 0} \frac{f^{(1)}(\eta+h)-f^{(1)}(\eta)}{h} \\ &= \lim_{h\to 0} \frac{f(\eta+2h)-2f(\eta+h)+f(\eta)}{h^2}, \end{aligned} \tag{18}$$

etc.

In general

$$\begin{aligned} f^{(n)}(\eta) &= D^n f(\eta) \\ &= \lim_{h\to 0} \frac{1}{h^n} \sum_{k=0}^{n} (-1)^k \binom{n}{k} f(\eta - kh), \end{aligned} \tag{19}$$

where,

$$\binom{n}{k} = \frac{n!}{k!(n-k)!}, \tag{20}$$

is a coefficient of a binomial. We can write a non-integer $\alpha > 0$ as

$$\binom{\alpha}{k} = \frac{\Gamma(\alpha+1)}{k!\,\Gamma(\alpha-k+1)}. \tag{21}$$

The Grünwald-Letnikov definition is the extension of the concept to a non-integer $\alpha > 0$

$$\begin{aligned} D_a^{\alpha} f(\eta) &= \lim_{h\to 0} \frac{1}{h^{\alpha}} \\ &\times \sum_{k=0}^{\frac{\eta-a}{h}} (-1)^k \frac{\Gamma(\alpha+1)}{k!\Gamma(\alpha-k+1)} f(\eta - kh). \end{aligned} \tag{22}$$

The fractional integral of order $\alpha > 0$ is given by

$$D_a^{-\alpha} f(\eta) = \lim_{h\to 0} \frac{1}{h^{\alpha}} \sum_{k=0}^{\frac{\eta-a}{h}} \frac{\Gamma(\alpha+1)}{k!\,\Gamma(\alpha)} f(\eta - kh). \tag{23}$$

2.1.3. Caputo fractional order derivatives

An illustration of a Caputo fractional order derivative is: Let $f \in C^n[a,b]$ and $n-1 < \alpha < n$ then

$$\begin{aligned} D_a^{\alpha} f(x) &= DI^{n-\alpha} D^n f(x) = \frac{1}{\Gamma(\alpha-n+1)} \\ &\times \int_a^x \frac{f^{(n)}(\eta)}{(x-\eta)^{\alpha-n+1}}\, d\eta; \quad a < x < b. \end{aligned} \tag{24}$$

Properties

$$D_a^{\alpha} C = 0, \tag{25}$$

$$\lim_{\alpha\to n} D_a^{\alpha} f(x) = f^{(n)}(x). \tag{26}$$

In this section, we present an algorithm for the estimation of Caputo fractional derivatives of any positive order $\alpha > 0$ for a given function. Our approach involves a weighted sum of the function and its ordinary derivative values at specified locations [14]. The foundation of our algorithm rests on the definition

$$\int_a^b f(\xi)\, d\xi \approx T(f,h), \tag{27}$$

where,

$$T(f,h) = \frac{h}{2}\left(f(a)+f(b)\right) + h\sum_{k=1}^{M-1} f(\xi_k). \tag{28}$$

This is an approximation to the integral of $f(\xi)$ over $[a,b]$. It is also based on a modified trapezoidal rule such that

$$T(f,h) = \frac{h}{2}\sum_{k=1}^{M}\left(f(\xi_{k-1})+f(\xi_k)\right). \tag{29}$$

In order to estimate the fractional integral $J^{\alpha} f(x)$ of order $\alpha > 0$, we present an adaptation of the trapezoidal rule (29).

Theorem 1. *Assume that the interval $[0,a]$ is partitioned into k equal-width sub-intervals $[x_j, x_{j+1}]$ of equal width $h = a/k$ using the nodes $x_j = jh$ for $j = 0,1,\ldots,k$. The revised trapezoidal rule is given by*

$$\begin{aligned} T(f,h,\alpha) &= \frac{(k-1)^{\alpha+1} - (k-\alpha-1)k^{\alpha}}{\Gamma(\alpha+2)} h^{\alpha} f(0) + \frac{h^{\alpha} f(a)}{\Gamma(\alpha+2)} \\ &+ \sum_{j=1}^{k-1} \frac{(k-j+1)^{\alpha+1} - 2(k-j)^{\alpha+1} + (k-j-1)^{\alpha+1}}{\Gamma(\alpha+2)} \\ &\times h^{\alpha} f(x_j). \end{aligned} \tag{30}$$

This approximation is close to the fractional integral operator

$$\begin{aligned} (J^{\alpha} f(x))(a) &= T(f,h,\alpha) - E_T(f,h,\alpha), \\ & a > 0, \quad \alpha > 0. \end{aligned} \tag{31}$$

Additionally, when $f(x) \in C^2[0,a]$, a constant C_a' exists that depends only on a, causing the error term $E_T(f,h,\alpha)$ to take the following form:

$$|E_T(f,h,\alpha)| \le C_a' \|f''\|_{\infty} a^{\alpha} h^2 = o(h^2). \tag{32}$$

Proof. As according to the fractional integral operator

$$J^{\alpha} f(x) = \frac{1}{\Gamma(\alpha)} \int_0^x (x-\tau)^{\alpha-1} f(\tau)\, d\tau, \quad x > 0, \tag{33}$$

we have

$$(J^{\alpha}f(x))(a) = \frac{1}{\Gamma(\alpha)}\int_0^a (a-\tau)^{\alpha-1}f(\tau)\,d\tau. \tag{34}$$

If $\tilde{f}_k$ is the piecewise linear interpolant for f with nodes picked at x_j, $j = 0, 1, 2, \ldots, k$, then by using the following equations:

$$\int_0^{t_k} (t_k - t)^{\alpha-1}\tilde{f}_k(t)\,dt = \sum_{j=0}^{k} a_{j,k} f(t_i), \tag{35}$$

where

$$a_{j,k} = \frac{h^{\alpha}}{\alpha(\alpha+1)} \begin{cases} (k-1)^{\alpha+1} - (k-1-\alpha)k^{\alpha}, & j = 0, \\ (k-j+1)^{\alpha+1} + (k-j-1)^{\alpha+1} - 2(k-j)^{\alpha+1}, & 1 \le j \le k-1, \\ 1, & j = k, \end{cases} \tag{36}$$

and

$$\left| \int_0^{t_k} (t_k - t)^{\alpha-1} f(t)dt - \sum_{j=0}^{k} a_{j,k} f(t_i) \right| \le C_{\alpha}\|f''\|_{\infty} t_k^{\alpha} h^2, \tag{37}$$

for some constant C_α depending only on α. We obtain

$$\int_0^a (a-\tau)^{\alpha-1}\tilde{f}_k(\tau)d\tau = \frac{h^{\alpha}}{\alpha(\alpha+1)}\Big[\left((k-1)^{\alpha+1} - (k-\alpha-1)k^{\alpha}\right) f(0) + f(a) + v\sum_{j=1}^{k-1}\left((k-j+1)^{\alpha+1} - 2(k-j)^{\alpha+1} + (k-j-1)^{\alpha+1}\right) f(x_j)\Big], \tag{38}$$

and

$$\left| \int_0^a (a-\tau)^{\alpha-1} f(\tau)d\tau - \int_0^a (a-\tau)^{\alpha-1}\tilde{f}_k(\tau)d\tau \right| \le C_{\alpha}\|f''\|_{\infty} a^{\alpha} h^2. \tag{39}$$

In this case, $C'_a = C_\alpha/\Gamma(\alpha)$. It is clear that the method's performance is unaffected by the parameter because it behaves quite similarly to the conventional trapezoidal rule. In particular, the modified trapezoidal rule (30) becomes the traditional trapezoidal rule (28) when $\alpha = 1$.

3. Material and methods

The materials, processes, and analytical techniques used in our inquiry of the radiation-induced changes in laboratory-grade ultra-high molecular weight polyethylene (UHMWPE) are covered in detail in this section. Our research started with the purchase of UHMWPE resin powder from Sigma-Aldrich, with an average molecular weight of between 3 and 6 million g/mol. A Gibitre laboratory press tool was used to further process the resin into sheets. Sheets were kept at temperatures of 150°C, 160°C, and 190°C for periods of 12-15 minutes at each of these temperatures while being formed under constant 200 bar pressures. After pressing, sheets were painstakingly cleaned using acetone to remove any potential impurities before being progressively cooled to ambient temperature (25°C) under sustained pressure. Each sheet was properly measured to have a thickness of about 1 mm using an internal reference point of the infrared (IR) vibration band at 2020 cm^{-1}. We described the UHMWPE material's physical and chemical characteristics, as shown in Table I, to give a thorough grasp of it. Its physical characteristics, empirical formula, density ρ, melting temperature, molecular weight, melt flow rate (MFI), and physical condition were all included in this list of characteristics.

The UHMWPE sheets were then exposed to gamma radiation in order to investigate any structural alterations. Two radiation doses of 50 kGy and 25 kGy (chosen due to their importance in the radiation sterilization of medical devices made of UHMWPE) were administered in an open-air setting with a regulated temperature of 25°C. Pakistan Radiation Services Lahore supplied the Co-60 gamma source, which had a constant dosage rate of 1.02 kGy/h. Each sheet was given a designation for easy identification, consisting of the letter "P" followed by the absorbed dose values (P-50, P-25, and P-0). Analytical methodologies focused on certain

TABLE I. Caputo fractional order derivative rule 800-1100 (50 kGy).

Differential Order	k	h	$C(f,h,\text{order})$	$E_c(f,h,\text{order})$
0th	31.0000	10.0000	10.8159	9.9699
0.5th	31.0000	10.0000	3.3898	2.5437
0.7th	31.0000	10.0000	2.0653	1.2192
0.8th	31.0000	10.0000	1.5879	0.7418
0.9th	31.0000	10.0000	1.2062	0.3601
1st	31.0000	10.0000	0.9037	0.0576

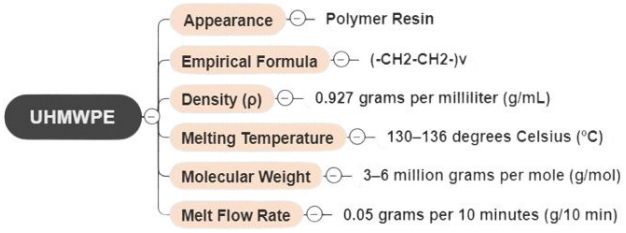

FIGURE 1. Characteristics of ultra-high molecular weight PE.

portions of the IR spectra associated with structural alterations were employed to assess radiation-induced changes in UHMWPE. These regions included the absorption of vinyl and trans-vinyldene at 800-1100 cm^{-1}, compounds with -C=O functional groups at 1600-1800 cm^{-1}, and changes within the UHMWPE structure at 3300-3600 cm^{-1}. The regions of interest in the IR spectra were carefully analysed after the experimental observations, where the regions of interest were plotted against the wavenumber, and the % transmittance data was calculated. Our inquiry into the effects of gamma radiation on UHMWPE was built on the foundation of these techniques and studies. To remove unwanted background noise and quasi-static signals from the data, the experimental spectra were carefully examined, and a variety of differential filters with fractional orders ranging from 0 to 1 were selectively applied. The dataset includes extra spectra produced using fractional order differential transformations (including 1st, 0.9th, 0.8th, 0.7th, and 0.5th orders) in addition to the original experimental spectra (treated as order 0). The primary objective of the study is to retain as much meaningful information as possible from the original experimental data, thus preferring lower fractional order differential transformations. Subsequently, to simulate fractional derivatives ranging from 0 to 1, a custom MATLAB function was developed employing the classical Grünwald-Letnikov definition, which incorporates the Lagrange-operator-based law to describe the rate of change at a given fractional order. Notably, these calculations are confined to the range of $0 < \alpha < 1$ (the fractional order) with an initial condition of $a = 0$, facilitating a comprehensive exploration of complex physical processes through the analysis of fractional derivatives. The Grünwald-Letnikov definition is the extension of the concept to a non-integer $\alpha > 0$.

$$D_a^{\alpha} f(\eta) = \lim_{h\to 0}\left(\frac{1}{h^{\alpha}}\sum_{k=0}^{\frac{\eta-a}{h}}(-1)^k \times \frac{\Gamma(\alpha+1)}{k!\Gamma(\alpha-k+1)} f(\eta-kh)\right). \quad (40)$$

Additionally, we used the Caputo fractional derivative definition with the trapezoidal rule to examine the precision and inaccuracy related to several fractional orders, namely 0.5th, 0.7th, 0.9th, 0.8th, and 1st-order, thereby adapting the approach to the unique properties of FTIR data. In practice, this involved creating unique MATLAB scripts capable of computing the Caputo fractional derivatives for various orders, offering a broad range of fractional order analysis. Through these calculations, we were able to quantify the errors associated with each fractional order, which provided insight into the validity of fractional order derivatives for interpreting FTIR data.

$$\int_a^b f(\xi)\, d\xi \approx T(f,h). \quad (41)$$

The simulation of fractional derivatives (FD) using Fourier Transform Infrared (FTIR) spectroscopic data served as the foundation for our work. To do this, we made use of the mathematical technique known as the Caputo fractional derivative definition, which is useful for describing complex behaviours in scientific datasets. To be more precise, we used FD to evaluate how FTIR data behaved at various fractional orders, including the 1st-order and the orders of 0.5, 0.7, 0.8, and 0.9. The trapezoidal rule was utilized as a computation method for precise FD calculations. This phase was crucial because it allowed us to determine which modifications to the FTIR spectra we could make while retaining the essential data. Additionally, it enabled us to observe the minute patterns and nuances that were concealed in the data. Following the simulation of the Fractional Derivative (FD), we computed correlation coefficients (CCs) using the formula provided below. This step aimed to identify the most suitable transformation method that minimizes information loss [15].

$$CC(XY) = \frac{\sum_{i=1}^{n}(X_i-\bar{X})(Y_i-\bar{Y})}{\sqrt{\sum_{i=1}^{n}(X_i-\bar{X})^2\sum_{i=1}^{n}(Y_i-\bar{Y})^2}}. \quad (42)$$

Here, $\bar{X}$ and $\bar{Y}$ are the mean values of the two parameters. The $CC(XY)$ range is from $+1$ to -1.

In addition to the aforementioned point-to-point correlation study of simulated data, we used Principal Component Analysis (PCA) to investigate how data dispersion varies when different orders of differential filters are applied. PCA is a dimension reduction technique that converts original data into new, uncorrelated variables called Principal Components. These components capture the most variance in the data, providing insights into hidden patterns, dynamics, and correlations. It also standardizes variables for comparing data dispersion. The original variables are divided into new components in this sort of analysis by axis rotation in PCA, which aids in identifying influential aspects in the composition of a sample. PCA produces a compact representation of the statistical relationships in the data with minimal information loss in terms of the order of differential transformation. The PCA equation is as follows:

$$Z_{ij} = a_{i1}x_{1j} + a_{i2}x_{2j} + \cdots + a_{im}x_{mj}, \qquad (43)$$

where,

- Z_{ij} denotes the component score.
- a_{ik} denotes the component loading.
- x_{kj} is the variable's measured value.
- i denotes the component number.
- j denotes the sample number.
- m represents the total number of variables.

For the analysis of the simulated FD data, we showed the score values (for each sample in all regions of interest) pertaining to the first two principal components. The primary goal of this work was to discover the similarities and differences between each UHMWPE sample across all three zones of interest, as well as to calculate the linkages between individual clusters.

4. Results and discussion

4.1. Experimental results

Shown in Fig. 2 is the IR spectra of UHMWPE. The absorption behaviour of UHMWPE has been studied for gamma-irradiation with dose values of 25 and 50 kGy. Due to physical and chemical changes brought on by radiation, there was a noticeable shift in the sample's absorbance. Significant changes are observed in the FTIR spectra due to the irradiation of the sample and thermal annealing. These changes are mainly due to C=C unsaturation absorption, C=O carbonyl absorption, and increased CH_2 bending and stretching frequencies, respectively. The results show the polyethylene IR band characteristics, which include -CH_2 stretching vibrations at 2849 and 2924 cm^{-1}, -CH_2 bending vibrations at

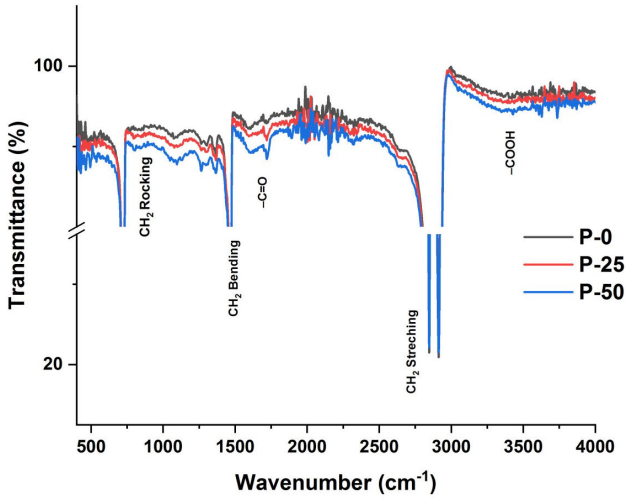

FIGURE 2. FTIR spectra of 0, 25, and 50 kGy irradiate with labelled functional groups of interest.

1490 and 1500 cm^{-1}, and -CH_2 rocking deformation at 717 and 730 cm^{-1}. A more detailed analysis of this spectrum revealed transitions in the regions 1450-1480 cm^{-1}, 1650-1850 cm^{-1}, 2800-2950 cm^{-1}, and 3000-3750 cm^{-1}. These regions correspond to -CH_2 bending, vibration, and absorption due to the unit -CH_2 in the amorphous region, and -C=O absorption, and -CH_2 stretching vibrations in the peroxide region. The surface alterations in peroxide-related products, *i.e.*, 3000-3750 cm^{-1}, and the absorption owing to -C=O in the range 1650-1850 cm^{-1} are essentially minimal for a gamma dose of 0 kGy; here, zero means that there was no oxidation in this sample.

The situation is substantially different for samples that have been exposed to radiation, since the radiation-caused free radicals lead the samples to undergo several chemical and physical changes. These free radicals have a variety of effects, such as forming crosslinks, breaking more P-E chains, and reacting with dispersed oxygen in the PE matrix after the well-known oxidation chain reactions of PE. Additionally, the amount of free radicals changes throughout all regions in a linear relationship with the concentrated gamma dosage, *i.e.*, -CH_2 bending vibration. The major affected areas that are strongly altered by irradiation treatment are the infrared regions between 800 cm^{-1} and 1100 cm^{-1}, and 1650 cm^{-1} and 1850 cm^{-1} in irradiated materials. The conversion of C=C unsaturated bonds into vinylidene ($R_1R_2C{=}CH_2$) and trans-vinylene (-CH=CH-) is responsible, and the presence of carbonyl C=O species, resulting from radiation-induced oxidation reactions, are responsible for the aforementioned alterations [16-20].

4.2. Simulated fractional order derivatives

Subsequent to the step-by-step procedure detailed in Sec. 3, MATLAB was employed to preprocess experimental spectral data and to apply fractional order differential transformations. The major ranges of interest (800-1100 cm^{-1}, 1700-1750 cm^{-1}, and 3300-3600 cm^{-1}) were analysed and are

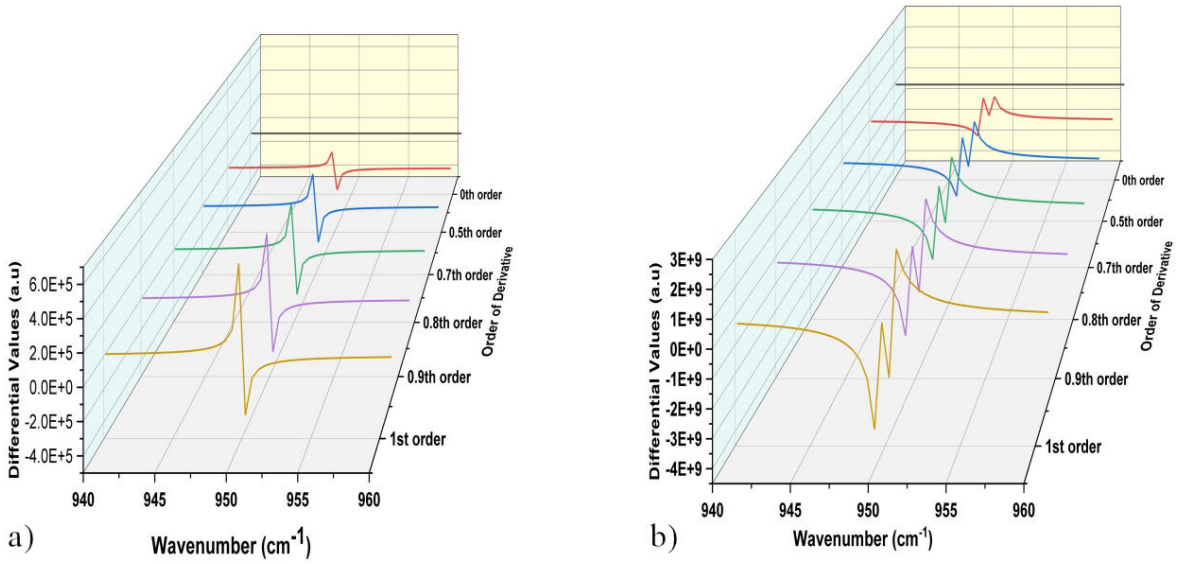

FIGURE 3. Simulated Fractional order and 1st-order derivative plots from 940-960 cm^{-1} a) for P-25, and b) P-50.

presented in Fig. 3. The data subsequent to transformation showed significant increases in differential maxima and minima corresponding to higher transformation orders and absorbed doses, indicating notable spectral changes. Specific spectral regions exhibited well-defined singular peaks that are crucial for identifying molecular vibrations and chemical bonds. The 800-1100 cm^{-1} range revealed peaks related to vibrational modes of chemical groups, the 1700-1750 cm^{-1} range to functional groups, and the 3300-3600 cm^{-1} range to hydrogen bonding and molecular interactions. The trend of increasing differential values with radiation dose highlighted the impact of gamma radiation on UHMWPE; leading to the formation of oxidation products and hydro-peroxides, which is evident in all corresponding figures. From the results, a peak splitting was observed in the 800-1100 cm^{-1} region for samples irradiated with 50 kGy. This split peak is attributed to the conversion of vinyl groups into vinylidene and trans-vinylene groups, thus confirming the effectiveness of applying fractional order differential transformation on the FTIR spectroscopy. This summarizes the fact that differential filtering improved the detection of trans-vinylene even at lower transformation orders, though the validity of each transformation order remains under investigation. However, a comprehensive assessment of the sensitivity and specificity of transformation orders using point-to-point linear correlations and principal component analysis (PCA) is given in subsequent sections for confidence on the accuracy of transformations [16,19-23].

4.3. Sensitivity and specificity analysis of fractional orders

4.3.1. Correlation index based sensitivity analysis

In our study, it's noteworthy that the correlation coefficients (CCs) for the experimental data, particularly the 0th-order spectrum, exhibit higher strength. However, our primary objective is to delve into the behaviour of CCs after the application of differential filters, as this is central to our investigation. To ensure a robust quantitative analysis of the alterations in spectra induced by radiation within the UHMWPE matrix, pinpointing the most responsive order of differential transformation is crucial for refining our analytical model. To address this, we performed a detailed analysis of point-to-point linear correlations between wavenumbers and differential values for each transformation order for all three regions of interest (800-1100 cm^{-1}, 1700-1750 cm^{-1} and 3300-3600 cm^{-1} respectively) as shown in Fig. 4 (D-F). The CCs were calculated using the method described in Sec. 3 of our study. Figure 4 depicts the strength of these CCs in a parallel plot format for each wavenumber, allowing for a visual assessment of point-to-point correlations between experimental and simulated fractional data. The convergence and strength of the CC distribution provide useful insights in such graphical representations. A more coherent and robust CC distribution implies less effect from quasi-static and background noise, with little loss of critical information during experimental spectral data translation, and vice versa. Our analysis of Fig. 4 reveals a compelling trend: the CCs are notably stronger for the differential transformation of the 0.5th-order and this trend holds across all three regions of interest. Furthermore, as we venture into higher orders of differentiation this heightened strength remains consistent. These findings underscore the suitability of lower-order differential filters, specifically the 0.5th-order utilized in our study. This choice is substantiated by the robust and coherent distribution of CCs across the spectral regions of interest. It reinforces the notion that employing lower-order differential filters enhances the precision and reliability of our model, allowing us to capture crucial information while mitigating the influence of undesirable noise. This in turn contributes to a more

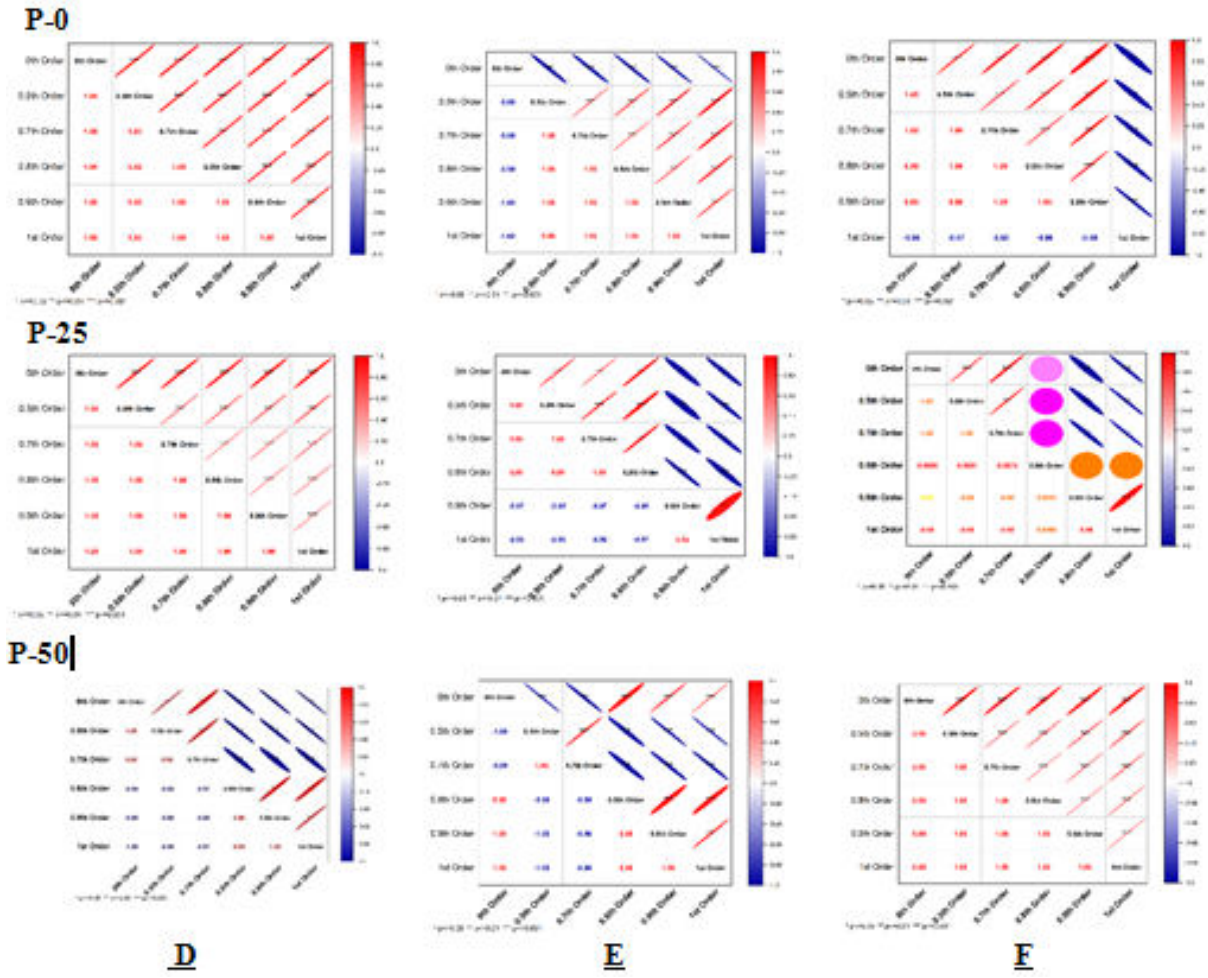

FIGURE 4. Point-to-point correlation coefficients for experimental and simulated FD spectral data for D) 800-1100 cm^{-1}, E) 1680-1800 cm^{-1}, and F) 3300-3600 cm^{-1}.

comprehensive and meaningful analysis of our data, a critical aspect of our study in evaluating radiation-induced modifications in UHMWPE.

4.3.2. Principal component analysis

Principal Component Analysis (PCA) of spectral data (experimental and simulated FD) was performed to confirm the sensitivity of the order of differentiation. The data dispersion for an unirradiated UHMWPE sample is presented as score plots on the first two principal components for all spectral regions of interest (see Fig. 5G)-I)). The PCA analysis provided the following significant insights. In our comprehensive analysis, we harnessed the power of Principal Component Analysis (PCA) to delve into the sensitivity of various fractional orders (1st-order and 0.5th, 0.7th, 0.8th, 0.9th) within the spectral confines of 800-1100 cm^{-1}, 1680-1800 cm^{-1}, and 3300-3600 cm^{-1} with a focus on the 800-1100 cm^{-1} (P-0 sample). The calculated ratios along both the x and y axes of these PCA results have shed light on the nuanced behaviours of these orders. What emerges as particularly intriguing is the 0.5th-order, which exhibits a remarkable equilibrium in sensitivity. This equilibrium is eloquently captured by its x-axis ratio of 1.29 and y-axis ratio of -0.79. Essentially, the 0.5th-order adeptly captures and balances the variance along both principal components, effectively preserving the entirety of the spectral characteristics. This characteristic sets it apart from the others, which demonstrate varied degrees of sensitivity and often accentuate a single principal component disproportionately. For instance, take the 1st-order, which, while displaying substantial sensitivity along the y-axis (ratio: 5.02), paradoxically exhibits an almost negligible influence along the x-axis (ratio: -0.02), potentially leading to a skewed representation of the data. Our findings highlight the practical utility of the 0.5th-order, mirroring the original unprocessed data (0th-order, x-axis value: 16.05, y-axis value: -4.84) with remarkable fidelity. This underscores the 0.5th-order's role as the preferred choice for meticulous scrutiny of radiation-induced modifications in UHMWPE, within the spectral ranges of 800-1100 cm^{-1}, 1700-1750 cm^{-1}, and 3300-3600 cm^{-1}, offering a harmonious blend of data refinement and unwavering fidelity to experimental observations.

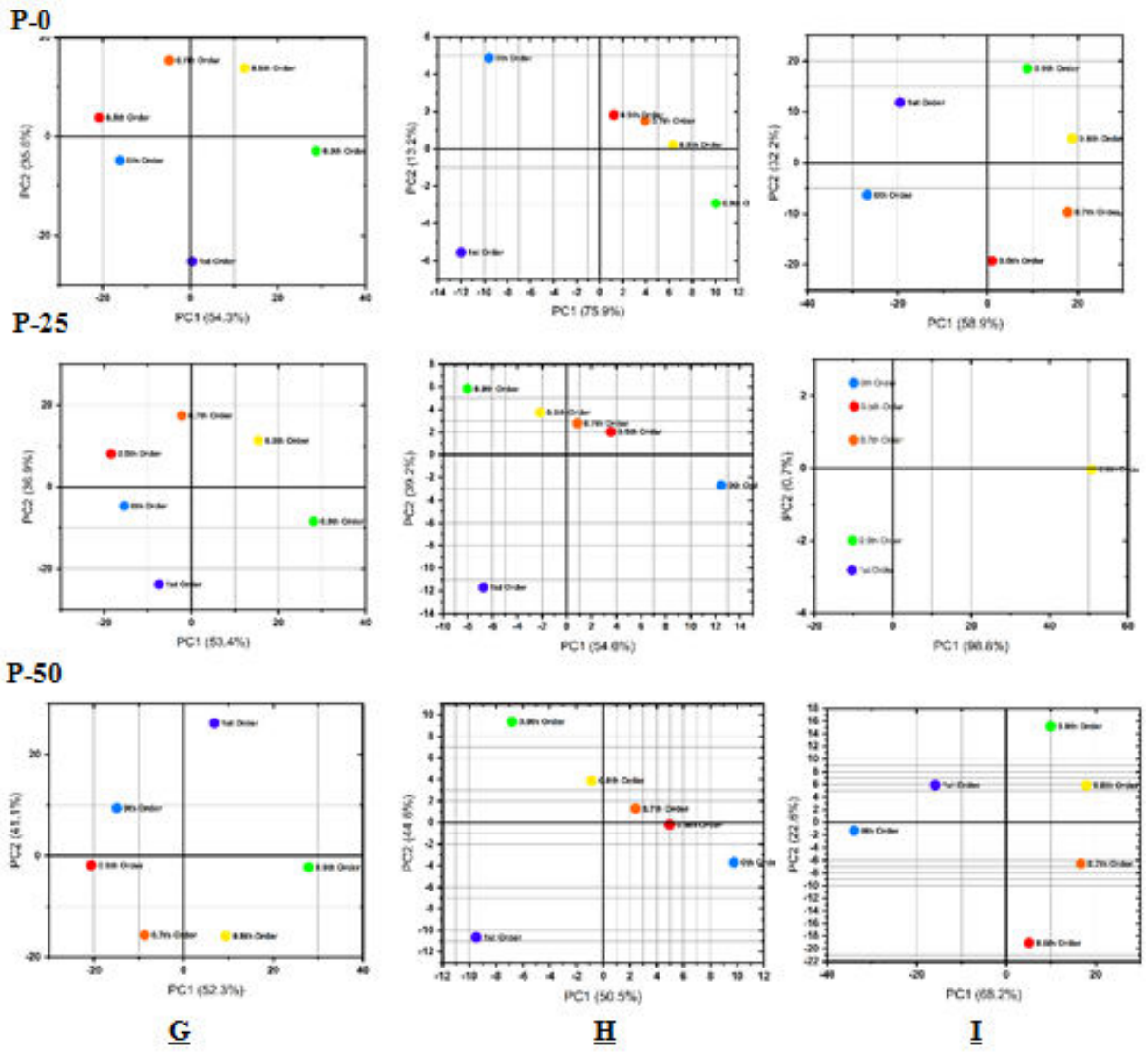

FIGURE 5. Principal Component Analysis of experimental and simulated FD spectral data for G) 800-1100 cm^{-1}, H) 1680-1800 cm^{-1} and I) 3300-3600 cm^{-1}.

4.3.3. Absolute value error analysis

In order to determine the spectral changes caused by 50 kGy radiation in Ultrahigh Molecular Weight Polyethylene (UHMWPE), we performed a careful analysis of Caputo fractional derivatives in three critical spectral regions: (800-1100 cm^{-1}, 1700-1750 cm^{-1} and 3300-3600 cm^{-1} respectively). These locations were chosen for their unique insights into the irradiation response of UHMWPE. Our primary focus was to assess the sensitivities of various fractional orders (1st-order and 0.5th, 0.7th, 0.8th, 0.9th) in capturing the essential spectral characteristics. Examining Table I, representing the 800-1100 cm^{-1} region, we observed how each fractional order deviated from the unirradiated 0th-order. No-

TABLE II. Caputo fractional order derivative rule 1700-1750 (50 kGy).

Differential Order	k	h	$C(f,h,\text{order})$	$E_c(f,h,\text{order})$
0th	6.0000	10.0000	-7.4539	8.3000
0.5th	6.0000	10.0000	-2.2632	3.1093
0.7th	6.0000	10.0000	-1.2669	2.1129
0.8th	6.0000	10.0000	-0.9137	1.7598
0.9th	6.0000	10.0000	-0.6370	1.4831
1st	6.0000	10.0000	-0.4240	1.2701

TABLE III. Caputo fractional order derivative rule 3300-3600 (50 kGy).

Differential Order	k	h	$C(f,h,\text{order})$	$E_c(f,h,\text{order})$
0th	30.0000	10.0000	1.8232	0.9772
0.5th	30.0000	10.0000	1.3191	0.4730
0.7th	30.0000	10.0000	1.2278	0.3817
0.8th	30.0000	10.0000	1.1527	0.3066
0.9th	30.0000	10.0000	1.0634	0.2173
1st	30.0000	10.0000	0.9650	0.1190

tably, the 0.5th-order displayed remarkable proximity to the 0th-order, marked by a Caputo fractional derivative (C) value of 3.3898, indicating a minimal shift due to radiation. The low absolute error (Ec) value of 2.5437 further underscored its accuracy in spectral preservation. A similar trend was observed in Table II, encompassing the 1700-1750 cm^{-1} region where the 0.5th-order again excelled with a C value of -2.2632 and an Ec value of 3.1093 signifying its precision in minimizing radiation-induced spectral shifts. This trend extended to Table III, representing the 3300-3600 cm^{-1} region where the 0.5th-order closely approximated the 0th-order with a C value of -0.6370 and an Ec value of 1.4831. Collectively, these results consistently showcased the 0.5th-order as the optimal choice for meticulous analysis providing an unrivalled balance between data refinement and faithfulness to experimental observations.

5. Conclusion

We used fractional differential transformation techniques ranging from 0.5th to certain infrared (IR) spectral bands of UHMWPE ranging from (800-1100 cm^{-1}, 1680-1800 cm^{-1}, and 3300-3600 cm^{-1}) and able to detect and distinguish the absorption signals of relatively weak bands associated with vinylidene (R1R2C=CH2) and trans-vinylene (-CH=CH-) groups in the 50 kGy irradiated UHMWPE. This demonstrates the utility of using differential transformation for figuring out the spectral information with minimal transformational loss as point-to-point correlation analysis and PCA confirmed that lower-order transformation is sufficient for spectral analysis with confidence. The fact stated above is also confirmed by the absolute error values, underscoring the 0.5th order's precision in preserving spectral integrity. In summary, our research demonstrates that fractional differential transformation, even at lowest order (0.5th in this particular study), is a valuable tool for accurately characterizing and quantifying radiation-induced changes in UHMWPE samples, enhancing our understanding of how this material responds to radiation exposure. The insights gained from this study hold promise for a wide range of applications, including materials science and medical device development, where the effects of radiation exposure on UHMWPE are of paramount importance. This research serves as a valuable foundation for future investigations and applications of irradiated UHMWPE materials.

Conflicts of Interest

All of the authors disclose that they do not have any competing interests.

Funding Specifics

This work got no funding.

Data Accessibility

On reasonable request, the corresponding author will provide any or all of the data, models, or code that support the findings of this work.

Contributions of authors

Each author made an equal contribution

1. L. Silva, Q. Martins, A. Ribas, D. Oliveira, R. Lima, and J. Santos, Raman and FTIR spectroscopy experimental and theoretical in magnetic nanoemulsion from Carapa Guianensis Aublet, *Rev. Mex. Fis.*, **69** (2023) 051003, https://doi.org/10.31349/RevMexFis.69.051003
2. A. Souigat, Z. Korichi, and M. T. Meftah, Solution of the fractional diffusion equation by using Caputo-Fabrizio derivative: application to intrinsic arsenic diffusion in germanium, *Rev. Mex. Fis.* **70** (2024) 010501 1, https://doi.org/10.31349/RevMexFis.70.010501.
3. M. Irfan *et al*., Raman spectroscopy and electrical properties of polypyrrole doped dodecylbenzene sulfonic acid/Y2O3 composites, *Rev. Mex. Fis.* **70** (2024) 010502 1, https://doi.org/10.31349/RevMexFis.70.010502.
4. M. M. Saeed, M. S. Mehmood, and M. Muhammad, Spectroscopic analysis of residual radicals of gamma sterilized

UHMWPE with fractional order differential operators, *Rev. Mex. Fis.* **70** (2024) 011001, https://doi.org/10.31349/RevMexFis.70.011001.

5. M. S. Mehmood *et al*., Assessment of γ-sterilization and/or cross linking effects on orthopedic biomaterial using optical diffuse reflectance spectroscopy, *Optik* **144** (2017) 387, https://doi.org/10.1016/j.ijleo.2017.06.127.
6. M. S. Mehmood *et al*., UHMWPE band-gap properties-II: Effect of post e-beam irradiation real time shelf aging in air, *Radiat. Phys. Chem.* **159** (2019) 231, https://doi.org/10.1016/j.radphyschem.2019.02.045.
7. M. S. Mehmood *et al.*, Mueller matrix polarimetry for characterization of E-Beam irradiated Uhmwpe, *Radiat. Phys. Chem.* **166** (2020) 108503, https://doi.org/10.1016/j.radphyschem.2019.108503.
8. R. Caponetto, Fractional order systems: modeling and control applications. (World Scientific, 2010). https://doi.org/10.1142/7709.
9. A. A. Kilbas, H. M. Srivastava, and J. J. Trujillo, Theory and applications of fractional differential equations. (Elsevier, 2006).
10. S. Saberhaghparvar and H. Panahi, Initial value problem for a Caputo space-time fractional Schrödinger equation for the delta potential, *Rev. Mex. Fis.* **68** (2022) 040703, https://doi.org/10.31349/RevMexFis.68.040703.
11. C. Li, D. Qian, Y. J. D. D. i. N. Chen, and Society, *On Riemann-Liouville and caputo derivatives*, **2011** (2011) 562494, https://doi.org/10.1155/2011/562494.
12. A. Atangana and J. F. Gómez-Aguilar, Numerical approximation of Riemann-Liouville definition of fractional derivative: From Riemann-Liouville to Atangana-Baleanu, *Numer. Methods Partial Differ. Equ.* **34** (2018) 1502, https://doi.org/10.1002/num.22195.
13. D. A. Murio, Stable numerical evaluation of Grünwald-Letnikov fractional derivatives applied to a fractional IHCP, *Inverse Problems in Science and Engineering*, **17** (2009) 229, https://doi.org/10.1080/17415970802082872.
14. Z. Odibat and Computation, *Approximations of fractional integrals and Caputo fractional derivatives*, **178** (2006) 527, https://doi.org/10.1016/j.amc.2005.11.072.
15. W. Jiang, C. Huang, and X. Deng, A new probability transformation method based on a correlation coefficient of belief functions, *Int. J. Intell. Syst.* **34** (2019) 1337, https://doi.org/10.1002/int.22098.
16. M. S. Mehmood, A. Sanawar, N. Siddiqui, and T. J. P. B. Yasin, *Quantification of silane grafting efficacy, weak IR vibration bands and percentage crystallinity in post e-beam irradiated UHMWPE*, *Polym. Bull.* **74** (2017) 213, https://doi.org/10.1007/s00289-016-1709-0.
17. M. S. Khurshid, M. S. Mehmood, and M. Zubair, Ultrahigh Molecular Weight Polyethylene and Graphene Oxide (UHMWPE/GO) Nano-composites for EMI Shielding, in Handbook of Polymer and Ceramic Nanotechnology: (Springer, 2021), pp. 1243-1267. https://doi.org/10.1007/978-3-030-40513-782.
18. M. S. Mehmood and M. N. Mehmood, Ultrahigh Molecular Weight Polyethylene and Silane (UHMWPE/Silane) Hybrids: Radiation Modifications and Characterization, in Handbook of Polymer and Ceramic Nanotechnology: (Springer, 2021), pp. 1377-1393. https://doi.org/10.1007/978-3-030-40513-784.
19. M. Slouf *et al*., *Structural changes of UHMWPE after e-beam irradiation and thermal treatment*, **85** (2008) 240, https://doi.org/10.1002/jbm.b.30942.
20. L. Costa, I. Carpentieri, P. J. P. D. Bracco, and Stability, Post electron-beam irradiation oxidation of orthopaedic Ultra-High Molecular Weight Polyethylene (UHMWPE) stabilized with vitamin E, *Polym. Degrad. Stab.* **94** (2009) 1542, https://doi.org/10.1016/j.polymdegradstab.2009.04.023.
21. L. Costa, I. Carpentieri, P. Bracco, Post electron-beam irradiation oxidation of orthopaedic UHMWPE, *Polym. Degrad. Stab.* **93** (2008) 1695, https://doi.org/10.1016/j.polymdegradstab.2008.06.003.
22. S. Liu *et al*., *Study on the post-irradiation oxidation of polyethylenes using EPR and FTIR technique*, *Polym. Degrad. Stab.* **196** (2022) 109846, https://doi.org/10.1016/j.polymdegradstab.2022.109846.
23. M. M. Saeed, M. Muddassar, M. S. Mehmood, H. M. J. R. P. Musharaf, and Chemistry, Diffuse reflectance spectroscopy of γ-irradiated UHMWPE: A novel fractional order based filters approach for accessing the radiation modification, *Radiat. Phys. Chem.* **197** (2022) 110163, https://doi.org/10.1016/j.radphyschem.2022.110163.